Detection of invisible phonon modes in individual defect-free carbon nanotubes by gradient-field Raman scattering*

Feng Yang(杨丰)[1,3,4], Yinglu Ji(纪英露)[2,‡], Xiao Zhang(张霄)[1,4], Qingxia Fan(范庆霞)[1,4], Nan Zhang(张楠)[1,4], Xiaogang Gu(谷孝刚)[1,3,4], Zhuojian Xiao(肖卓建)[1,3,4], Qiang Zhang(张强)[1,4], Yanchun Wang(王艳春)[1,3], Xiaochun Wu(吴晓春)[2,4], Junjie Li(李俊杰)[1], and Weiya Zhou(周维亚)[1,3,4,†]

[1] *Beijing National Laboratory for Condensed Matter Physics, Institute of Physics, Chinese Academy of Sciences, Beijing* 100190, *China*
[2] *National Center for Nanoscience and Technology, Beijing* 100190, *China*
[3] *Beijing Key Laboratory for Advanced Functional Materials and Structure Research, Beijing* 100190, *China*
[4] *University of Chinese Academy of Sciences, Beijing* 100049, *China*

(Received 14 April 2017; published online 6 June 2017)

We provide an effective method to investigate the field gradient effect in nanoconfined plasmon–matter interaction. Aligned ultralong SWNTs without defects were grown on marked substrates, followed by assembling gold nanoparticle clusters around individual nanotubes. The Raman scattering behavior of a nanotube placed in an atomic scale nanogap between adjacent nanoparticles was studied. In addition to the expected plasmon-induced Raman enhancement up to 10^3, the defect-free D-mode of an individual SWNT induced by gradient field is found for the first time. When the light is confined at atomic scale, gradient field Raman scattering becomes significant and dipole-forbidden phonon modes can be activated by quadrupole Raman tensor variation, indicating breakdown of the Raman selection rules.

Keywords: carbon nanotube, Raman scattering, electromagnetic field gradient, selection rule

PACS: 88.30.rh, 36.20.Ng, 78.67.Pt, 76.60.Gv **DOI:** 10.1088/1674-1056/26/7/078801

1. Introduction

Surface plasmons, collective oscillations of conduction band electrons in metal nanostructures, exhibit an extraordinary ability to route and manipulate light on sub-diffraction limits with intense electromagnetic (EM) field.[1] The field enhancement mechanism offers unique opportunities for enhancing signals in a series of spectroscopic techniques. For instance, vibrational modes of molecules situated at the surface of these metallic nanostructures have been strengthened by several orders of magnitude, well-known as surface enhanced Raman scattering (SERS).[2] SERS is a powerful analytical technique owing to its low detection limits to probe molecular fingerprints. In the conditions of huge field enhancement, detections at the single-molecule level have been reported.[3]

It is generally accepted that the EM enhancement mechanism (scaling as the fourth power of the local EM field amplitude), caused by the enhanced near field generated by exciting the plasmon, contributes the largest enhancements. The other mechanisms such as chemical enhancement are responsible for only a small part of the total enhancement. Beyond the EM enhancement mechanism, the effect of EM gradient-field becomes significant when the EM field is confined to an atomic dimension (several ångströms).[4] Raman scattering caused by the gradient field (i.e., the gradient-field Raman scattering, GFR), which differs appreciably from the normal Raman scattering in selection rules, has been widely discussed since the 1980s both in theory and experiments.[5,6] In a normal Raman process, the EM field generally couples to the dipole transition moment in electronic excitation, that is, the dipole–dipole polarizability derivative governs the scattering, so the higher order contributions can be neglected. However, if a field gradient presents at atomic scale, there are photon states excited through the quadrupole transition moment. In that case, Raman scattering could arise from the dipole–quadrupole and quadrupole–quadrupole polarizability derivatives, which should lead to changed selection rules.[4]

Owing to their well-known optical and vibrational properties,[7,8] single-walled carbon nanotubes (SWNTs) are suitable target materials for studying GFR. Furthermore, SWNTs are chemically inert. Deposition of nanotubes aqueous suspension onto the substrate with metallic nanostructures has been used to assemble nanoplasmon-nanotube systems,[9,10] but it is still difficult to construct an ideal interface between an atomic scale near-field hotspot and an individual SWNT. Considering their straight profile and homogeneous properties along the nanotube axis, aligned ultralong SWNTs are more competent for placing an individual SWNT in a nanoconfined field. Moreover, it is easier to compare

*Project supported by the National Basic Research Program of China (Grant No. 2012CB932302), the National Natural Science Foundation of China (Grant Nos. 11634014, 51172271, and 51372269), and the "Strategic Priority Research Program" of the Chinese Academy of Sciences (Grant Nos. XDA09040202 and XDA09040400).

†Corresponding author. E-mail: wyzhou@iphy.ac.cn
‡Corresponding author. E-mail: jiyl@nanoctr.cn

© 2017 Chinese Physical Society and IOP Publishing Ltd

the intrinsic and enhanced Raman signals from an individual SWNT.

In this work, we present an effective method to investigate the GFR in nanoconfined plasmon-matter interaction. Aligned individual ultralong SWNTs were grown on marked substrates by gas flow guiding chemical vapor deposition (CVD)[11] and followed by assembling gold nanoparticles with a given diameter around individual SWNTs. Then nanogaps can be obtained to confine the EM around individual SWNTs at several ångströms scale due to the hexagonal close-packing of nanoparticles.[12] Raman spectra of individual SWNTs in the nanogaps were collected before and after the nanoparticles assembly at the same position with respect to the markers on the substrate. In addition to the considerable Raman enhancement by the EM mechanism, significant D-band in defect-free SWNTs was also found in this system. It indicates that the Raman scattering selection rules were changed by the field gradient.

2. Experimental section

2.1. Preparation of aligned SWNTs

Ultralong, well-aligned SWNTs were grown on marked substrates by a CVD technique similar to the previous work of our group.[13] Hemoglobin (Hb) solution (1 mg/ml) was used as the catalyst precursor and spincoated on a silicon wafer (with a 500 nm thick thermally oxidized layer) and then annealed in air at 800 °C for 5 min. The annealed catalyst was pretreated at 850 °C in Ar and H_2 (30% H_2 by volume) ambiance for 5 min to reduce the catalyst. Aligned SWNTs were grown by introduction of 10 sccm H_2 and 5 sccm CH_4 at 950 °C on a silicon wafer (with a 500-nm-thick thermally oxidized layer) as the receiving substrate, etched with 300 nm deep trenches by reactive ions as markers. After 50 min of growth, the substrate with aligned SWNTs, protected by H_2, was cooled down to room temperature.

2.2. Synthesis and assembly of gold nanoparticles

Gold nanoparticles (Au NPs) with a mean diameter of $\sim$ 30 nm were synthesized by a seed-mediated method.[14] The precipitates with 30 nm-Au NPs, after centrifugation (8000 rpm for 5 min), were collected and redispersed with 50 mL deionized water.

A drop of diluted Au NPs suspension was placed onto a marked substrate with aligned SWNTs. Followed by 30 min baking under incandescence, the hexagonal close-packed nanoparticle clusters after drying and nanogaps between the nearest neighbor nanoparticles were formed around individual SWNTs.

2.3. Characterizations

The diameter, morphology, and microstructures of as synthesized SWNTs and nanoparticles were characterized by scanning electron microscope (SEM, Hitachi 4800) and transmission electron microscope (TEM, Tecnai F20).

The sample was illuminated by a white light from a photonic-crystal-fiber laser. A 100×, NA 0.9, and IR-corrected microscope objective was used to collect the scattered light that is directed to a spectrometer. A charge coupled device (CCD) detector was used to obtain the dark field spectra in the visible range. The spectra were acquired at isolated plasmonic clusters to avoid contributions from other clusters.

Raman spectra of SWNTs were recorded using micro-Raman spectroscopy (HORIBA JY, HR800) with 1800 grating (0.65 cm^{-1} accuracy) and a 100× objective (NA = 0.9), resulting in a laser spot size of about 1 μm. For laser excitation radiation, the 514 nm (2.41 eV) line from an Ar^+ laser and the 785 nm (1.58 eV) line from a solid state Al-doped GaAs laser were adopted. Through an optical attenuation slice, about 1 mW power for the two lasers was reached at the sample surface, with no obvious additional Raman shift and irradiation damage caused by the laser heating. The polarization direction for the incident light was controlled via an achromatic $\lambda/2$ plate.

3. Results and discussion

Figure 1(a) shows the SEM image of as-grown well-aligned SWNTs on a marked substrate (left) and the magnification of a segment of the individual SWNT (right). Owing to the low flow rate feeding, the Reynolds number of the gas flow is very small. So floating SWNTs can be well aligned by stable laminar flow in the growth process.[11] A defined rectangular coordinate is shown in Fig. 1(a), in which the y axis is parallel to the tube axis. It is the polarization direction selected for the incident light in order to obtain considerable intrinsic Raman signals.[15]

Figure 1(b) shows the Raman spectra of the SWNT excited by 514 nm and 785 nm laser, respectively. The latter was multiplied by 3 for better comparing the two Raman spectra. The strongest G-band around 1580 cm^{-1} is from the G-phonons near the Γ point of the Brillouin zone (BZ) and is always regarded as the fingerprint of sp^2 orbital hybridization of carbon materials.[8] Figures 1(c) and 1(e) are G-band maps of the SWNT excited by these two lasers, respectively. Homogeneous G-bands along the y axis certify the consistency of vibrational properties of the SWNT.

The D-band in the range of 1250–1400 cm^{-1} is a second-order double resonance Raman scattering mode in SWNTs and other graphene based carbon materials, which arise from phonons near the K point of the BZ (also called noncentral

phonon mode). Its frequency depends on the photon energy of the incident laser.[16,17] An elastic scattering between the photon and defect in SWNTs is needed in the double resonance Raman scattering process to obey the momentum conservation law, so the intensity of the D-band (normalized to G-band) is a quantization factor of disorders in SWNTs. The D-band is centered at 1350 cm^{-1} and 1300 cm^{-1} for 514 nm laser and 785 nm laser, respectively.[8] The absence of a D-band in the two spectra excited by two different lasers, as shown in Fig. 1(b), indicates that the SWNT is free of defects. For further ensuring the absence of defects, corresponding D-band maps along the *y* axis are shown in Figs. 1(d) and 1(f).

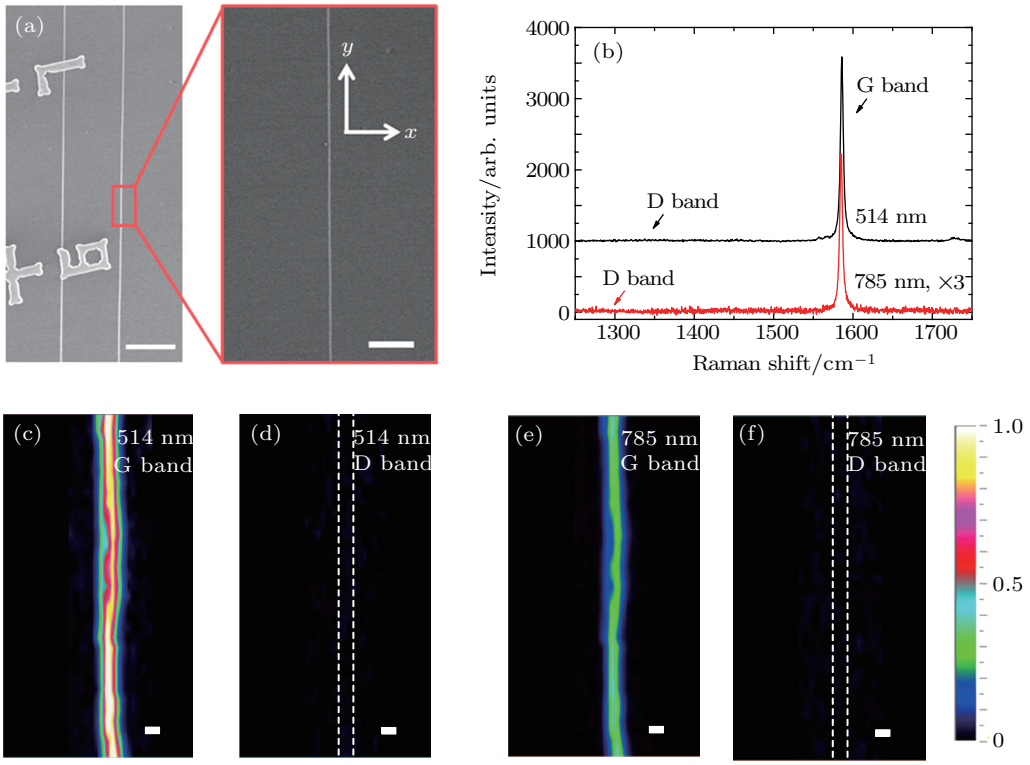


Fig. 1. (color online) (a) SEM images of as-grown SWNTs, the right enlarged image shows the SWNT, in which the coordinate illustrates the *x* and *y* direction defined in this paper. The scale bars are 20 μm and 1 μm, respectively. (b) Raman spectra of the SWNT with the laser along the *y*-axis polarization. (c)–(f) G-band maps and D-band maps of the SWNT excited by 514 nm laser and 785 nm laser, where the double dashed lines denote the position of the SWNT. The scale bars in these maps are 500 nm.

Au NP (with a diameter of ∼ 30 nm) clusters assembled on marked substrate are used to enhance the Raman signals of the SWNT. A typical TEM photograph of 30 nm Au NPs shown in Fig. 2(a) demonstrates that the Au NPs are spherical polyhedrons. After dropping to the substrate, Au NPs attract each other due to van der Waals interaction and other attractive forces during the evaporation of water. The gaps between neighboring Au NPs become narrower by baking using an incandescent lamp.

Figure 2(b) is an SEM image of the cluster and the SWNT. Once Au NPs assemble as a hexagonal close-packed cluster around the SWNT, nanogaps are formed between adjacent NPs. Because of the polyhedral shape of NPs, the dimension and shape of nanogaps might be diversified on the substrate: nanogaps ranging from a few ångströms to several dozen ångströms can be found in this system. It is known that the incident EM field is localized in these nanogaps with high intensity and great field gradient could be produced due to tiny gaps,[9,12] called hotspots. Owing to various morphologies of nanogaps and the straight profile of individual ultralong SWNTs, this system is a suitable model for investigating the GFR effect.

Figure 2(c) is the dark field spectra collected from the isolated Au NP cluster shown in Fig. 2(b). The optical response of the plasmonic cluster exhibits collective behavior on account of the strong coupling effect between neighboring Au NPs.[18] The scattering maximum locates at 750 nm in our experimental range. As we know, the near-field resonance of plasmonic structures is red shifted compared to the scattering maximum,[19] thereby providing a good match with an excitation of 785 nm. As a contrast, the 514 nm laser is out of plasmon resonance range.

In the following, the Raman response of the SWNT coupled with the Au NP cluster was characterized. With an excitation of 514 nm laser, no Raman enhancement from the cluster occurs. Figure 3(a) shows the Raman spectra of the SWNT with *y*-direction polarized incident laser ($\boldsymbol{P}_y$, red curve) and *x*-direction polarized incident laser ($\boldsymbol{P}_x$, black curve), consistent

with the intrinsic Raman spectra collected on the bare substrate (see Fig. 1(b)). Absorption and emission of light perpendicular to the tube axis is strongly suppressed by depolarization effect,[15] so no Raman signal appears for $\boldsymbol{P}_x$. The intensity ratio of G-band $I(P_x)/I(P_y) < 0.05$, calculated by integrated peak areas, is a characteristic feature for Raman scattering of SWNTs. It is noticeable that no D-band appears in both spectra, confirming the perfect crystal structure of the SWNT.

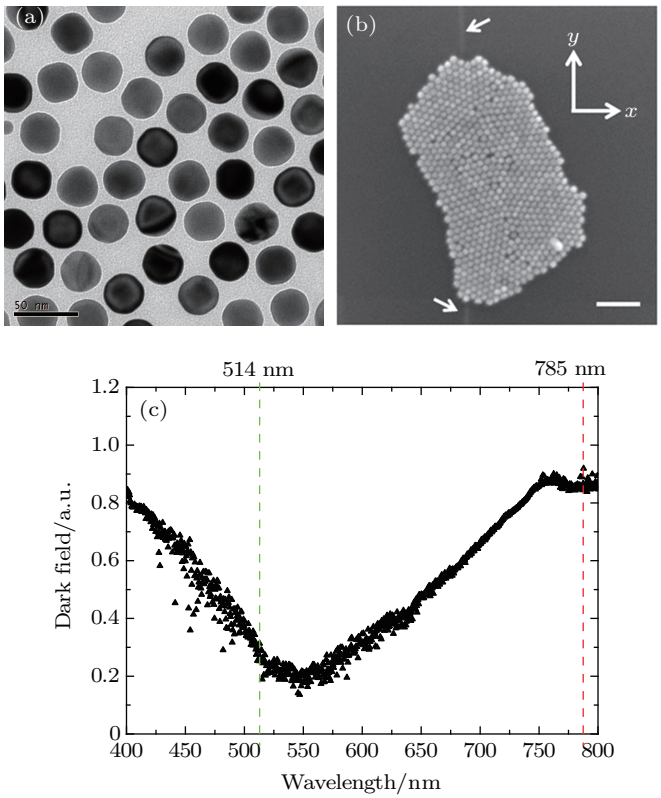


Fig. 2. (color online) (a) TEM image of 30 nm Au NPs. The scale bar is 50 nm. (b) SEM image of a SWNT covered by Au NP cluster, in which the white arrows denote the position of the SWNT. The scale bar is 200 nm. (c) Dark field spectrum of the cluster shown in panel (b).

Figure 3(b) shows the Raman spectra of the SWNT for $\boldsymbol{P}_y$ (red curve) and $\boldsymbol{P}_x$ (black curve) excited by 785 nm laser. For the presence of SERS enhancement, drastic changes are observed in the Raman response of the SWNT. The Raman signature for $\boldsymbol{P}_y$ is consistent with the intrinsic one (see Fig. 1(b)), where no enhancement from the cluster occurs. For $\boldsymbol{P}_x$, however, the Raman intensity is greatly enhanced, demonstrated by the high intensity ratio of G-band $I(P_x)/I(P_y) \approx 25$. Compared with the normal Raman process (the D- and G-peak intensity ratio < 0.05), it is a sign of the enhancement by localized surface plasmons which has been investigated in carbon nanotubes coupled with polarization sensitive plasmonic structures.[9,20] Similar to the small carbon nanotube bundles coupled with plasmonic nanodisk dimers reported by Heeg *et al.*,[9] the dominating surface plasmon excitation in the cluster investigated here is of dipolar nature, leading to high near-fields localized in the nanogaps. If we take the enhanced field area into account, the enhancement factor for $\boldsymbol{P}_y$ is on the order of magnitude of 10^3.

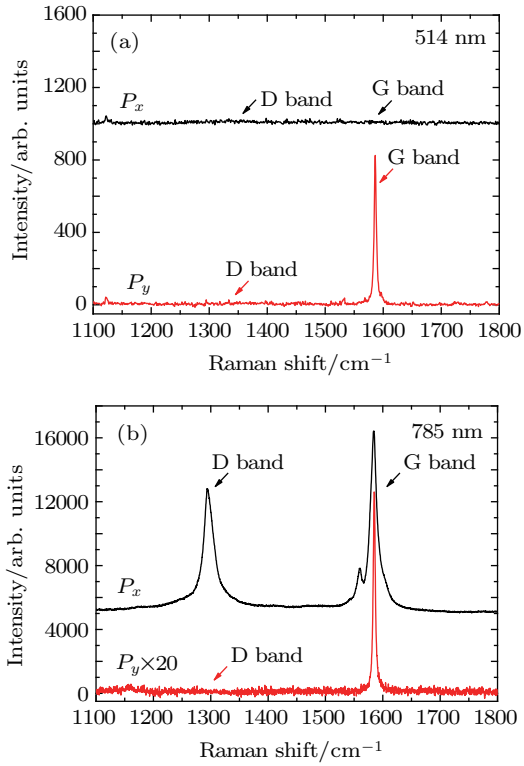


Fig. 3. (color online) Raman spectra of the SWNT coupled with Au NP cluster shown in Fig. 2(b), excited by 514 nm laser (a) and 785 nm laser (b), respectively.

More interestingly, in addition to the noticeable SERS enhancement along the x direction, a strong D-band without defect is also found in the Raman spectra for $\boldsymbol{P}_x$, which has not been reported elsewhere. The relative intensity of D-band $I(D)/I(G) \approx 0.73$, is far greater than the intrinsic one (< 0.05).

Further plasmon-induced Raman scattering in an individual SWNT coupled with Au NP clusters are investigated using the same method as mentioned above. A defect-free D-band arises in some of clusters with different relative intensity (varying from 0.15 to 1), although in other clusters, no observable D-band is detected in SWNTs without defect, similar to conventional plasmonic enhancement. This means that the relative intensity of defect-free D-band depends on the nanogap dimension. This phenomenon is strong evidence to prove the presence of GFR at ångström scale plasmon-induced Raman scattering, in which the Raman selection rule should have a change induced by the field gradient effect.

To confirm that the D-band does not arise from laser induced defects, the Raman response of SWNTs was characterized after Au NP clusters removed by deionized water. Figure 4 shows the SEM image and corresponding Raman spectra of the SWNT after the rinse process. The absence of a D-band ensures that the band arises from GFR instead of defects.

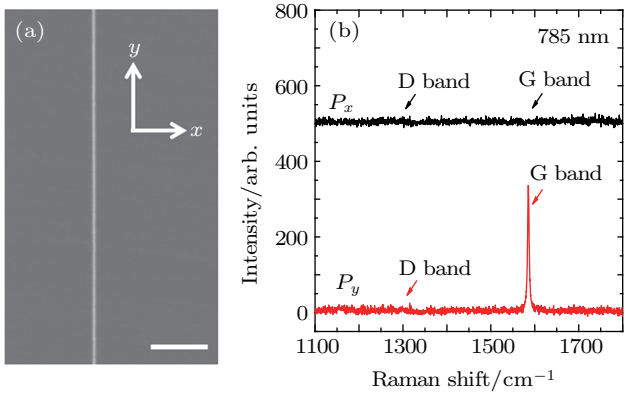


Fig. 4. (color online) (a) SEM image of the SWNT after the Au NP cluster was removed by water. The scale bar is 500 nm. (b) The corresponding Raman spectra of the SWNT shown in (a).

As mentioned above, the D-band is a noncenter phonon mode beyond the Γ point in BZ and is forbidden in the conventional Raman process in defect-free SWNTs. From the viewpoint of the selection rules for Raman scattering, the activation of the noncenter phonon modes in the absence of defects indicates the selection-rule breakdown in the Raman scattering process and has not been reported in carbon nanotubes before.

For an SWNT placed in an EM field, the dipole moment μ in the coordinate of vibration q can be written as[4]

$$\mu_a = \left[\left(\frac{\partial \mu_a^p}{\partial q}\right)_0 + \left(\frac{\partial \alpha_{ab}}{\partial q}\right)_0 E_b + \left(\frac{\partial E_b}{\partial q}\right)_0 \alpha_{ab} + \frac{1}{3}\frac{\partial E_b}{\partial c}\left(\frac{\partial A_{abc}}{\partial q}\right)_0\right] q + o\left(q^2\right), \quad (1)$$

where $\{a,b,c\}$ is a permutation of the coordinates $\{x,y,z\}$ and summing over repeated indices is implied, $\boldsymbol{\alpha}$ and $\boldsymbol{A}$ are the polarizability tensors, and $\boldsymbol{E}$ is the electric field. The first and second terms result in infrared absorption and Raman scattering, respectively. The last two terms correspond to the contribution of field gradients to Raman scattering, which are negligible in a conventional Raman process based on the long wavelength approximation.

According to group theory of SWNTs, G-band and D-band are classified as $\Gamma - E_{2g}$ phonon mode and $K - A_1'$ phonon mode, respectively.[21,22] The second term is responsible only for activation of the G-mode under the dipole approximation in a conventional Raman process. The fourth term in the above expression can activate the D-mode when the field variations are large enough. Typically, the nanogap dimension dropped down to several ångströms. Furthermore, the quadrupole tensor $\boldsymbol{A}$ for D-mode has a nonzero element of $A_{xxx} - 3A_{xxy}$, which can strongly boost the D-band.

Figure 5 shows the Raman process of D-mode in resonance Raman scattering (RRS) and GFR. In the RRS process, as shown in Fig. 5(a), the electron (1) absorbs a photon at a $\boldsymbol{k}$ state near the K point in BZ, the electron (2) scatters to $\boldsymbol{k}+\boldsymbol{q}$ state near the K' point in BZ, the electron (3) elastically scatters back to the $\boldsymbol{k}$ state with defect, and the electron (4) emits a photon by recombining with a hole at the $\boldsymbol{k}$ state.[8] Without the elastic scattering between the electron and defect, the D-mode is not directly detectable by optical excitation. Instead, in the case of the plasmon mediated GFR process, a defect-mediated elastic scattering is not needed for the momentum conservation, the nanoconfined light with larger $\boldsymbol{k}$ vectors makes nonvertical optical transition allowed,[23] the electron at the $\boldsymbol{k}+\boldsymbol{q}$ state in the conduction band can be scattered back to a $\boldsymbol{k}$ state in the valence band directly.

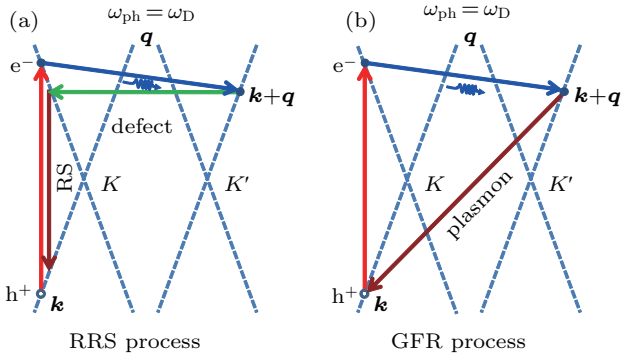


Fig. 5. (color online) Comparison of the activation process of the D-band between conventional and plasmonic excitation. (a) Conventional resonance Raman scattering (RRS) process. (b) Gradient-field Raman (GFR) process.

The GFR plays an important role in sub-nanometer scale light–matter interaction. Gradient field induced optical transition selection-rule breakdown in SWNTs has been reported by Takase *et al.*[10] For SWNTs in the gap of gold nanopyramid dimers, the high EM field gradient in the nanogap enables the observation of the forbidden transition E_{14}, indicating modification of electronic resonance selection rules. The breakdown of the Raman selection rules makes sub-nanometer plasmonic structures a powerful tool not only for enhancing photon–matter interaction efficiency, but also for tailoring the photon–matter interaction pathway.

4. Conclusion

The gradient-field Raman scattering of defect-free aligned individual SWNTs coupled with close packed gold nanoparticle clusters has been investigated. In addition to the considerable plasmon-induced Raman enhancement on the order of 10^3 arising from the EM enhancement mechanism, a strong D-band without defect is also found in this system when the nanogaps between neighboring nanoparticles are reduced to several ångströms scale. The relative intensity of plasmon-induced D-band varies from 0 to 1 in our experiment, sensitively depending on the nanogap dimension surrounding the SWNT. In a conventional resonance Raman process, an elastic scattering between the electron and defect in the SWNT is needed for the momentum conservation, so the D-mode is invisible in a defect-free SWNT. However, when the light

is confined at atomic scale in the nanogaps, GFR becomes significant and a defect-free D-mode can be activated by the quadrupole Raman tensor variation, indicating breakdown of the Raman selection rules.

References

[1] Barnes W L, Dereux A and Ebbesen T W 2003 *Nature* **424** 824

[2] Stiles P L, Dieringer J A, Shah N C and Van Duyne R R 2008 *Ann. Rev. Ana. Chem.* **1** 601

[3] Kneipp K, Wang Y, Kneipp H, Perelman L T, Itzkan I, Dasari R and Feld M S 1997 *Phys. Rev. Lett.* **78** 1667

[4] Ayars E J, Hallen H D and Jahncke C L 2000 *Phys. Rev. Lett.* **85** 4180

[5] Moskovits M and Dilella D P 1980 *J. Chem. Phys.* **73** 6068

[6] Sass J K, Neff H, Moskovits M and Holloway S 1981 *J. Phys.Chem.* **85** 621

[7] Dresselhaus M S and Eklund P C 2000 *Adv. Phys.* **49** 705

[8] Dresselhaus M S, Dresselhaus G, Saito R and Jorio A 2005 *Phys. Rep.* **409** 47

[9] Heeg S, Oikonomou A, Fernandez-Garcia R, Lehmann C, Maier S A, Vijayaraghavan A and Reich S 2014 *Nano Lett.* **14** 1762

[10] Takase M, Ajiki H, Mizumoto Y, Komeda K, Nara M, Nabika H, Yasuda S, Ishihara H and Murakoshi K 2013 *Nat. Photon.* **7** 550

[11] Jin Z, Chu H, Wang J, Hong J, Tan W and Li Y 2007 *Nano Lett.* **7** 2073

[12] McMahon J M, Li S, Ausman L K and Schatz G C 2012 *J. Phys. Chem. C* **116** 1627

[13] Zhang X, Yang F, Zhao D, Cai L, Luan P, Zhang Q, Zhou W, Zhang N, Fan Q, Wang Y, Liu H, Zhou W and Xie S 2014 *Nanoscale* **6** 3949

[14] Ma Y, Li W, Cho E C, Li Z, Yu T, Zeng J, Xie Z and Xia Y 2010 *Acs Nano* **4** 6725

[15] Duesberg G S, Loa I, Burghard M, Syassen K and Roth S 2000 *Phys. Rev. Lett.* **85** 5436

[16] Saito R, Jorio A, Souza A G, Dresselhaus G, Dresselhaus M S and Pimenta M A 2002 *Phys. Rev. Lett.* **88** 027401

[17] Kurti J, Zolyomi V, Gruneis A and Kuzmany H 2002 *Phys. Rev. B* **65** 165433

[18] Hentschel M, Saliba M, Vogelgesang R, Giessen H, Alivisatos A P and Liu N 2010 *Nano Lett.* **10** 2721

[19] Alonso-Gonzalez P, Albella P, Neubrech F, Huck C, Chen J, Golmar F, Casanova F, Hueso L E, Pucci A, Aizpurua J and Hillenbrand R 2013 *Phys. Rev. Lett.* **110** 203902

[20] Paradiso N, Yaghobian F, Lange C, Korn T, Schuller C, Huber R and Strunk C 2015 *Phys. Rev. B* **91** 235449

[21] Alon O E 2001 *Phys. Rev. B* **63** 201403

[22] Damnjanovic M, Milosevic I, Vukovic T and Sredanovic R 1999 *Phys. Rev. B* **60** 2728

[23] Beversluis M R, Bouhelier A and Novotny L 2003 *Phys. Rev. B* **68** 115433